ISPRS Journal of Photogrammetry and Remote Sensing 94 (2014) 80–90

Contents lists available at ScienceDirect

ISPRS Journal of Photogrammetry and Remote Sensing

journal homepage: www.elsevier.com/locate/isprsjprs

Soil respiration mapped by exclusively use of MODIS data for forest landscapes of Saskatchewan, Canada

Chaoyang Wu [a,b,*], David Gaumont-Guay [c], T. Andrew Black [d], Rachhpal S. Jassal [d], Shiguang Xu [a], Jing M. Chen [b], Alemu Gonsamo [b]

[a] State Key Laboratory of Remote Sensing Science, Institute of Remote Sensing and Digital Earth, Chinese Academy of Sciences, Beijing 100101, China
[b] Department of Geography, University of Toronto, 100 St. George St., Toronto, ON, Canada
[c] Biometeorology Research Laboratory, Vancouver Island University, Nanaimo, BC, Canada
[d] Faculty of Land and Food Systems, University of British Columbia, Vancouver, BC, Canada

ARTICLE INFO

Article history:
Received 4 March 2014
Received in revised form 17 April 2014
Accepted 21 April 2014
Available online 20 May 2014

Keywords:
Soil respiration
Forest
Soil temperature
Remote sensing
MODIS
NDVI
Land surface temperature

ABSTRACT

Soil respiration (R_s) is of great importance to the global carbon balance. Remote sensing of R_s is challenging because of (1) the lack of long-term R_s data for model development and (2) limited knowledge of using satellite-based products to estimate R_s. Using 8-years (2002–2009) of continuous R_s measurements with nonsteady-state automated chamber systems at a Canadian boreal black spruce stand (SK-OBS), we found that R_s was strongly correlated with the product of the normalized difference vegetation index (NDVI) and the nighttime land surface temperature (LSTn) derived from Moderate Resolution Imaging Spectroradiometer (MODIS) imagery. The coefficients of the linear regression equation of this correlation between R_s and NDVI × LSTn could be further calibrated using the MODIS leaf area index (LAI) product, resulting in an algorithm that is driven solely by remote sensing observations. Modeled R_s closely tracked the seasonal patterns of measured R_s and explained 74–92% of the variance in R_s with a root mean square error (RMSE) less than 1.0 g C/m^2/d. Further validation of the model from SK-OBS site at another two independent sites (SK-OA and SK-OJP, old aspen and old jack pine, respectively) showed that the algorithm can produce good estimates of R_s with an overall R^2 of 0.78 ($p < 0.001$) for data of these two sites. Consequently, we mapped R_s of forest landscapes of Saskatchewan using entirely MODIS observations for 2003 and spatial and temporal patterns of R_s were well modeled. These results point to a strong relationship between the soil respiratory process and canopy photosynthesis as indicated from the greenness index (i.e., NDVI), thereby implying the potential of remote sensing data for detecting variations in R_s. A combination of both biological and environmental variables estimated from remote sensing in this analysis may be valuable in future investigations of spatial and temporal characteristics of R_s.

1. Introduction

The interannual variability in net ecosystem production (NEP) has been mainly attributed to the direct effects of climate variability on CO_2 assimilation through gross primary photosynthesis (GPP) and CO_2 loss through ecosystem respiration (R_e) (Valentini et al., 2000; Wu et al., 2013a). Soil respiration (R_s), the flux of microbially- and plant-respired CO_2 from the soil surface to the atmosphere, is the second-largest terrestrial carbon (C) flux (Bond-Lamberty and Thomson, 2010), and therefore is considered as one of the most significant components of the global C balance (Högberg et al., 2001). Recent results of Wu et al. (2013a) even suggest that respiration process might be more important than photosynthesis in determination of interannual variability of C balance in forests.

R_s integrates several biological and physical processes, including the production of CO_2 by roots, mycorrhizal fungi, microorganisms and soil fauna throughout the soil profile, and the subsequent diffusion of CO_2 to the soil surface (Bond-Lamberty and Thomson, 2010; Gaumont-Guay et al., 2014). Seasonal variation in the ratio of R_s to R_e is constrained by the interactions among (a) phenological differences between aboveground and belowground plant tissues, (b) mobilization and use of stored substrates within woody plants, and (c) seasonal variation in photosynthate and litter substrates (Davidson et al., 2006). The rate of R_s is influenced by many

* Corresponding author at: State Key Laboratory of Remote Sensing Science, Institute of Remote Sensing and Digital Earth, Chinese Academy of Sciences, Beijing, 100101, China. Tel.: +10 64889215.
E-mail address: hefery@163.com (C. Wu).

http://dx.doi.org/10.1016/j.isprsjprs.2014.04.018
0924-2716/

factors, which generally can be classified into abiotic (e.g., soil water content, SWC) and biotic elements (e.g., canopy photosynthesis). There is considerable evidence that R_s is tied to soil temperature (T_s) across multiple spatial and temporal scales (Gaumont-Guay et al., 2006; Jassal et al., 2005; Jassal et al., 2012a). Consequently, T_s plays an important role in many models of soil CO_2 production (Reichstein et al., 2003; Jassal et al., 2004; Ngao et al., 2012). SWC is suggested to have a more complicated effect on R_s due to its strong link with soil-respiratory processes (Gaumont-Guay et al., 2006; Griffis et al., 2004). Although the effects of T_s and SWC on R_s cannot always be separated easily, the relative importance of the two factors may be different in various climate conditions (Ekblad et al., 2005). As R_s depends on the availability of organic substances respired by roots and microorganisms, photosynthetic activity supplying carbohydrates from leaves to roots and rhizosphere is also recognized as a key driver of R_s (Moyano et al., 2008; Kuzyakov and Gavrichkoa, 2010; Caquet et al., 2012). This conclusion is supported by correlations between R_e and GPP across land cover types (Yuan et al., 2009) as well as between R_s and photosynthesis-related vegetation indices (Huang et al., 2012; Bond-Lamberty et al., 2012; Jassal et al., 2012a). Therefore, these environmental and biological variables may potentially provide useful insights into modeling R_s.

Large scale quantification of R_s is a major challenge albeit we have long-term observations at many sites worldwide (Bond-Lamberty and Thomson, 2010) and fine spatial landcover information (Zhu and Toutin, 2013; Mitrakis et al., 2012). While a large dataset can provide a unique insight into R_s patterns and its changes with climate, it is still limited considering both temporal and spatial heterogeneity in physical and biochemical properties. For example, observations of R_s from the dataset of Bond-Lamberty and Thomson (2010) are at annual scale, making it impossible to analyze fine temporal (e.g., daily, monthly and seasonal) variations in R_s. Since an increasing number of global carbon cycling models include R_s as a model input (Blonquist et al., 2006; Mahecha et al., 2011), it is important if R_s can be modeled on the basis of remotely sensed data, which is also the most convenient way to investigate its spatiotemporal patterns. Such knowledge is useful in modeling ecosystem C changes over time and space (Trumbore, 2006; Bahn et al., 2010). Currently, there is no report on the operational use of R_s modeling based on remote sensing observations. One important reason is that long-term R_s measurement requires a great amount of field work and such long R_s record has not been accumulated sufficiently long to ensure a robust testing of algorithms. Recent analysis of Huang et al. (2012) show that the vegetation index derived from canopy measurements may be a good proxy of R_s. However, a limitation of these results is the inappropriate consideration of abiotic factors (e.g., temperature) that have been shown for long to have effects on R_s. Therefore, new algorithms are needed with reasonable parameterizations of both biotic and abiotic factors to estimate R_s and such efforts would be helpful for analyzing spatial and temporal patterns of R_s in future.

Using eight years (2002–2009) of soil CO_2 efflux measurements obtained with nonsteady-state automated chamber systems in a boreal black spruce stand (Jassal et al., 2012b; Gaumont-Guay et al., 2014), we propose a new approach to model R_s based entirely on remotely sensed imagery from the Moderate Resolution Imaging Spectroradiometer (MODIS). We further applied the model at other two forest sites (an evergreen needleleaf forest and a deciduous broadleaf forest) with independent chamber measurements. Finally, we mapped R_s of forest landscapes of the whole province using MODIS data and these efforts may serve as an important step in the investigation of spatial and temporal variability of R_s in future.

2. Materials and methods

2.1. Study sites

Three Boreal Forest Research and Monitoring Sites (BERMS) were used in this study, including (1) a mature aspen stand (SK-OAS, deciduous broadleaf forest), (2) a mature black spruce stand (SK-OBS, evergreen needleleaf forest) and (3) a mature jack pine stand (SK-OJP, evergreen needleleaf forest) (Black et al., 2000; Barr et al., 2004; Dunn et al., 2007; Zhang et al., 2009; Gaumont-Guay et al., 2009). These sites are located in the mid-boreal lowland ecoregion in the boreal plain ecozone near Prince Albert, Saskatchewan, Canada (Fig. 1). The climate of the region is typified by short, warm, dry summers and long, cold winters. These sites provide an opportunity to analyze R_s of contrasting species at different sites. Detailed site characteristics for each site are provided in Table 1.

2.2. MODIS data

Three land surface MODIS products were used and they were downloaded from the Oak Ridge National Laboratory's Distributed Active Archive Center (DAAC) website (http://www.modis.ornl.gov/modis/index.cfm). The first is the 8-day Terra MODIS surface reflectance product (MOD09A1, 0.5 km) that provides surface reflectance for seven wavelength bands (centered at 648, 858, 470, 555, 1240, 1640, and 2130 nm, respectively). Each pixel contains the best possible observation during an 8-day period as selected on the basis of high observation coverage, low viewing angle, the absence of clouds or cloud shadow, and aerosol loading (Justice et al., 2002). The reflectance for the first two wavelength bands were used to calculate the normalized difference vegetation index (NDVI) as,

$$\mathrm{NDVI} = (R_{NIR} - R_{Red})/(R_{NIR} + R_{Red}) \quad (1)$$

where R_{NIR} and R_{Red} represent the reflectance for the near-infrared (MODIS band 2) and red (MODIS band 1) wavelength bands (nm), respectively.

The second MODIS product is the 8-day Land Surface Temperature (LST) (MOD11A2, 1 km) derived by applying the generalized split-window algorithm (Wan, 2008). In the split-window algorithm, emissivities in bands 31 and 32 are estimated from land cover types, and atmospheric column water vapor and lower boundary air surface air temperature are separated into tractable sub-ranges for optimal retrieval (Wan, 2008). Both daytime and nighttime LST (referred as LSTd and LSTn, respectively, hereafter) were used in this study.

The third MODIS product is the 8-day leaf area index (LAI) product (MOD15A2, 1 km). LAI is defined as the one-sided green leaf area per unit ground area in broadleaf canopies and as half the total needle surface area per unit ground area in coniferous canopies (Chen et al., 1997). The MODIS LAI product is derived from the surface reflectance, the land cover type, and ancillary information on surface characteristics such as background (Myneni et al., 2002).

Based on the geo-location information of the site, NDVI was extracted from the 3×3 pixel area with its center point close to the flux tower (Xiao et al., 2004; Wu et al., 2011, 2014). For the LST (both LSTd and LSTn) and LAI products, we also used the values for the 3×3 pixels considering the seasonal variations of the flux footprints reported for these sites (>3 km^2, Chen et al., 2011) and previous C fluxes modeling approaches (Sims et al., 2008; Wu et al., 2012).

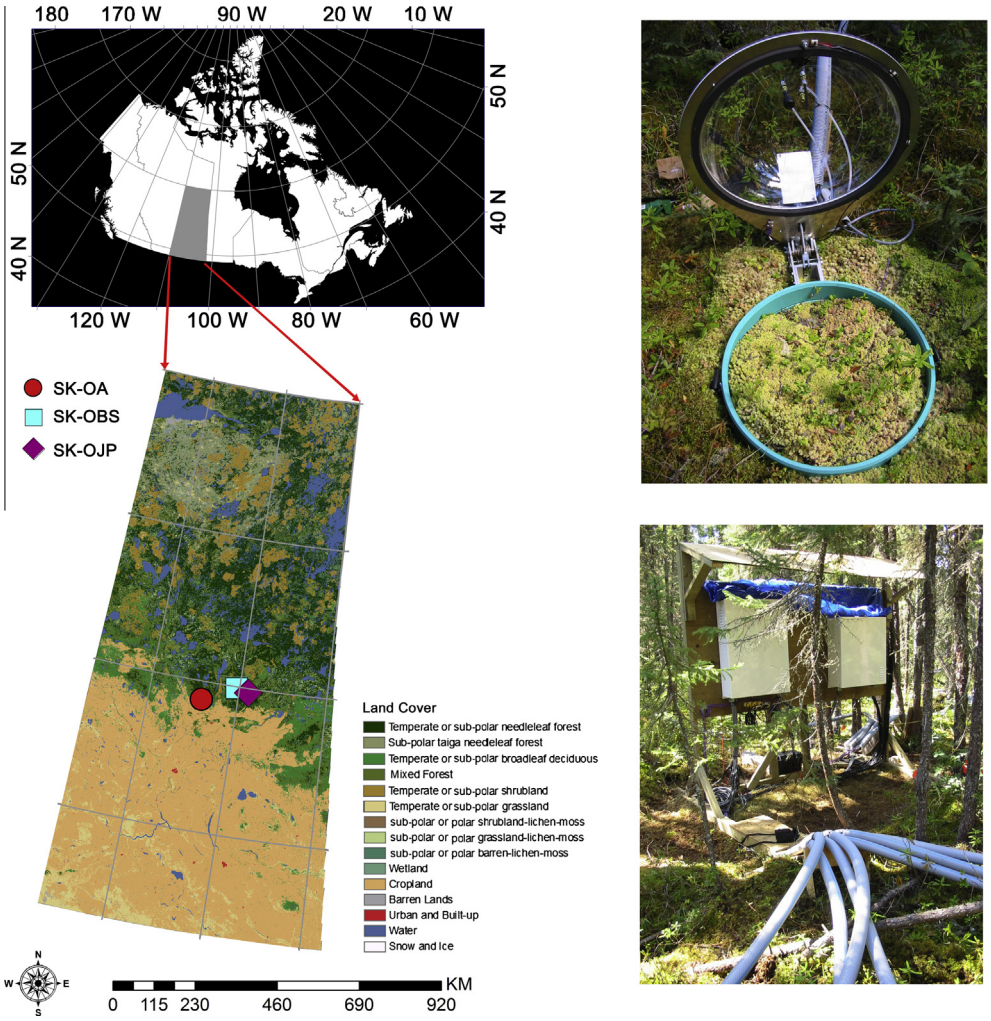

Fig. 1. Description of the study sites with land cover data and photos of ground measurements at SK-OBS site.

Table 1
Descriptions of site characteristics in this study.

Sites	Old black spruce (SK-OBS)	Old aspen (SK-OA)	Old jack pine (SK-OJP)
Location	53.99 N, −105.12 W	53.63 N, −106.20 W	53.92 N, −104.69 W
Plant functional type	Evergreen needle-leaf forest	Deciduous broad-leaf forest	Evergreen needle-leaf forest
Data range	2002–2009	2003	2003
Data usability	Modeling	Independent validation	Independent validation
Stand age (2012)	133	93	83
Dominant species	Black spruce, jack pine, tamarack	Trembling aspen, hazelnut	Jack pine, alder, lichen
Drainage[†]	Imperfect to poor	Well to moderately well	Very well
Mineral layer	Sandy clay	Loam to clay	Fine sand
Stand density (trees ha-1)	4330	980	1320
Tree height (m)	7.2	20.1	12.7
DBH (cm)	7.1	20.5	12.9

[†] Data from Gaumont-Guay et al. (2009).

2.3. Soil CO_2 efflux measurements

Similar nonsteady-state automated chamber systems were used to continuously measure soil CO_2 efflux at these three sites. Other variables such as near-surface soil temperature (T_s, 5-cm depth), volumetric soil water content (SWC, 7.5-cm depth) and radiation, were also measured. All chambers, which had a volume of approximately 60 L, were randomly located within a 25-m radius of temperature-controlled housings (TCHs) containing an infrared gas analyzer, pumping and data logging equipment. Each chamber consisted of a moveable transparent lid attached by hinges to a fixed collar inserted between 3 and 4 cm into the soil. The lids were kept open when the chambers were not in use to allow rain, snow and litter to fall into the collar area.

For SK-OBS site (modeling site), a long-term dataset was obtained during 2002–2009 (Gaumont-Guay et al., 2014). Two identical chamber systems were used during the eight years; the first system was used from 2002 to 2003 and the second system from 2004 to 2009. The total number of chambers used during the periods of 2002–2003, 2004–2006 and 2007–2009 were 5, 7 and 6, respectively. The forest-floor vegetation during the first measurement period contained the feather moss, herbaceous,

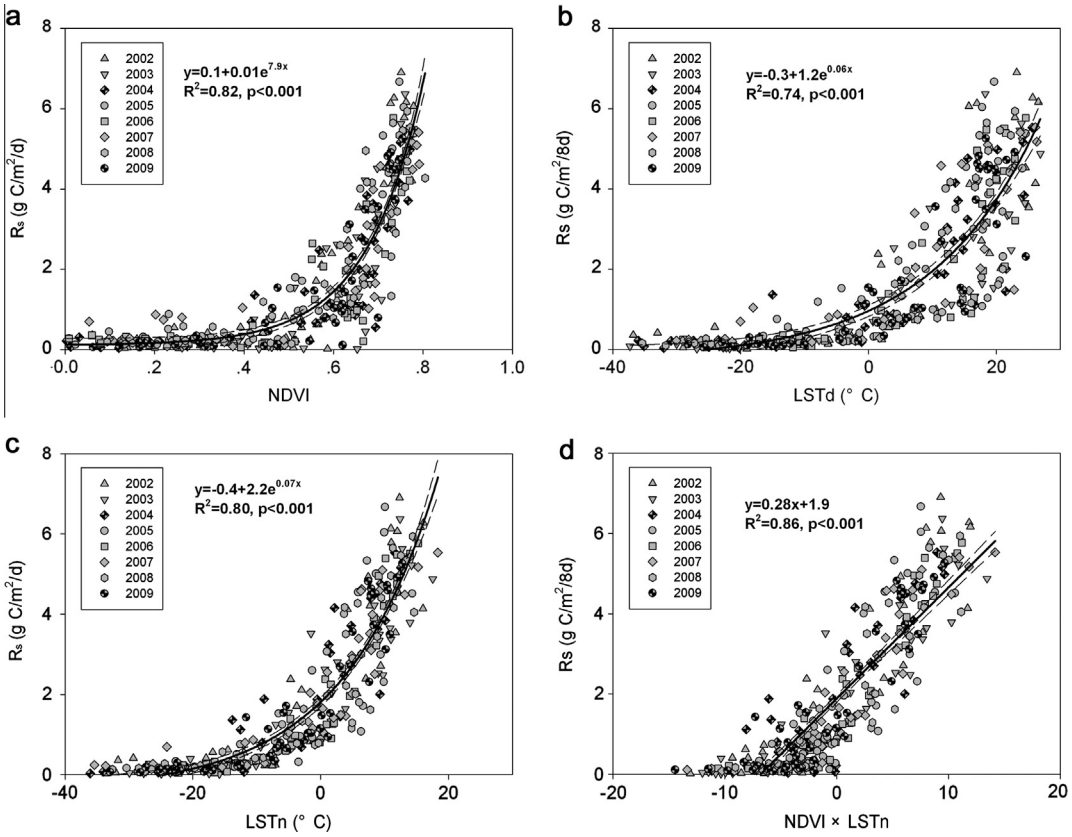

Fig. 2. Relationships between soil respiration (R_s) and (a) normalized difference vegetation index (NDVI), (b) daytime land surface temperature (LSTd), (c) nighttime land surface temperature (LSTn), and (d) product of the NDVI and LSTn (NDVI × LSTn) from 2002 to 2009. Each point is an 8-day average. The solid lines are the regression lines (equations shown in each panel) and the dashed lines are the 95% confidence intervals of mean prediction.

and hollow. Additional forest-floor vegetation, such as sphagnum, lichen, and mineral soil, were included during the second measuring period. For both SK-OA and SK-OJP, four soil chambers were used throughout 2003. For SK-OA, herbaceous plants growing in the collar area were clipped regularly to expose only the bare soil. For SK-OJP, three of the four chambers were used to represent the lichen community and the remaining one represented the mixed feather moss and lichen area. More detailed descriptions of ground measurements and instruments can be found in Gaumont-Guay et al. (2009).

Half-hourly soil CO_2 efflux, F_{cs} (μmol CO_2 m^{-2} s^{-1}), was calculated as:

$$F_{cs} = \rho_a \frac{V_e}{A} \frac{ds_c}{dt} \quad (2)$$

where ρ_a is the molar density of dry air (mol m^{-3}), V_e is the effective volume of the chamber (m^3), A is the area of ground covered by the chamber (m^2), $\frac{ds_c}{dt}$ is the time rate of change in the CO_2 molar mixing ratio (μmol CO_2 mol^{-1} dry air s^{-1}) following lid closure, and t is the time (s).

Half-hourly measurements from all chambers were averaged to obtain representative half-hour values and were then summed to acquire daily totals (Griffis et al., 2004; Gaumont-Guay et al., 2009). Considering that the remote sensing data provide observations at ecosystem scale (i.e., 1 km resolution), a scaling-up algorithm was used to scale the component fluxes of chamber measurements to ecosystem level according to the percent coverage of the forest-floor communities as descried in Bisbee et al. (2001) and Gaumont-Guay et al. (2014). In particular, previous results of Gaumont-Guay et al. (2014) at SK-OBS site showed that the data-scaling algorithm is independent on the time of data acquisition and did not introduce significant inaccuracies in the model development for R_s estimation.

2.4. Partitioning soil CO_2 efflux into R_s and P_{ff} at SK-OBS and SK-OJP

Considering the lids of chambers for soil CO_2 efflux measurements were transparent, which would allow radiation to reach the forest floor covered by a thick mat of feather and sphagnum mosses, for SK-OBS and SK-OJP, the half-hourly measured soil CO_2 efflux is the net forest-floor CO_2 exchange, which represents the balance between R_s (autotrophic (roots and mosses) and heterotrophic (microbial) respiration) and moss photosynthesis. For SK-OA, no contribution of forest-floor photosynthesis (P_{ff}) was observed since the chambers only included bare soil (Gaumont-Guay et al., 2009). Therefore, for the two evergreen needleleaf forest stands (SK-OBS and SK-OJP), procedures were needed to partition F_{cs} into R_s and P_{ff}.

To separate R_s from F_{cs}, we used the method proposed by Gaumont-Guay et al. (2014). Briefly, an exponential equation relating surface soil temperature (T_s, 5-cm depth) and the nighttime (below canopy $PAR_{1m} < 5$ μmol m^{-2} s^{-1}, P_{ff} equals to zero) half-hourly measured soil CO_2 efflux (i.e., nighttime soil respiration) was used to estimate daytime R_s,

$$F_{cs} = R_{10} Q_{10}^{(T_s - 10)/10} \quad (3)$$

where Q_{10} and R_{10} represent the temperature sensitivity coefficient and the base soil respiration at 10 °C (μmol m^{-2} s^{-1}), respectively. These parameters together with daytime T_s were used to model daytime R_s, and P_{ff} was then determined as the difference between measured F_{cs} and the modeled daytime R_s.

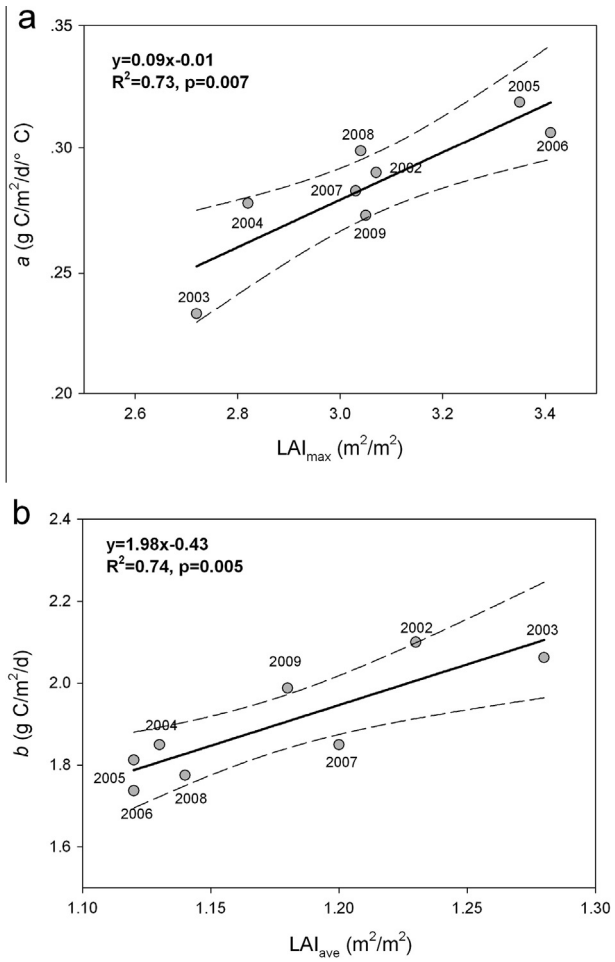

Fig. 3. Relationships between (a) the slope of the R_s-NDVI × LSTn regression (a) and the annual maximum leaf area index (LAI) and (b) between the intercept of the R_s–NDVI × LSTn regression (b) and the annual average LAI from 2002 to 2009. The dashed lines show the 95% confidence intervals of mean prediction for the regression line.

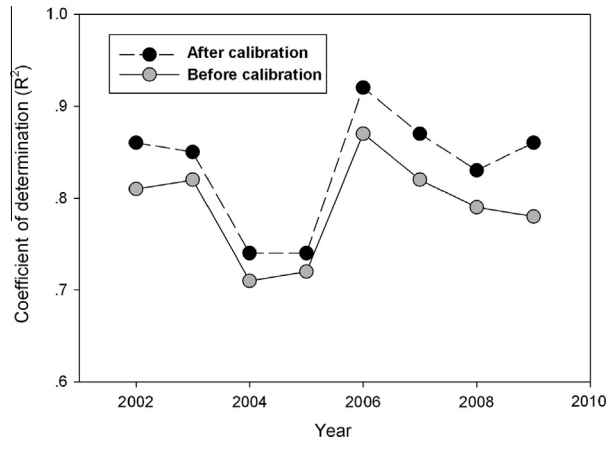

Fig. 4. Comparison between the coefficients of determination (R^2) before and after calibration, i.e., without and with parameterizing a (i.e., the slope) and b (i.e., the intercept) using statistics of LAI.

Gaps in the – P_{ff} record were filled using a rectangular hyperbolic function (Gaumont-Guay et al., 2009),

$$P_{ff} = \frac{\alpha P_{\mathrm{ffmax}} \mathrm{PAR}_{\mathrm{below}}}{\alpha \mathrm{PAR}_{\mathrm{below}} + P_{\mathrm{ffmax}}} \quad (4)$$

where α, P_{ffmax}, $\mathrm{PAR}_{\mathrm{below}}$ represent the apparent quantum use efficiency, the horizontal asymptotic value of P_{ff} and the below canopy radiation, respectively.

2.5. Modeling strategy

The objective of our analysis is to develop a new model that estimates R_s entirely based on MODIS data and to validate the model at independent sites. Since much longer dataset was available at SK-OBS site, we mainly focused on this site to develop the model and measurements from other two sites were then used for independent validation. Therefore, we first explored MODIS-derived NDVI and LST (both LSTd and LSTn) in their strength to explain R_s variations using 8 years of records at SK-OBS site. The evaluation was conducted considering that R_s was controlled by both biotic (e.g., photosynthesis) and abiotic factors (e.g., temperature). We then also calibrated the model, i.e., determining coefficients of regression, using MODIS observations (i.e., statistics of time series of LAI) to ensure that all inputs are from remote sensing data. In addition, we tested the general applicability of the model derived at SK-OBS site at another two sites of both deciduous broadleaf and evergreen needleleaf forests with independent measurements. Finally, we mapped R_s of forest landscapes (forest pixels were identified from the 2005 North American Land Cover at 250 m spatial resolution, http://www.cec.org/naatlas/) of the whole province of Saskatchewan with the algorithm using entirely MODIS data to show the spatial and temporal patterns of R_s. Since the MODIS LSTn had the lowest spatial resolution among all inputs of the algorithm (MODIS reflectance, LST and LAI products), the final R_s map was produced at 1 km spatial resolution monthly, which was summed from each 8-day simulation.

3. Results

3.1. Relationship between R_s and MODIS NDVI, LSTd and LSTn

We found that NDVI was an important driver of R_s explaining 82% of the variance in R_s in the black spruce stand, confirming the connection between belowground processes and photosynthetic activity (Fig. 2a). However, this connection seemed time dependent as NDVI was only useful in predicting R_s during the growing season, i.e. for NDVI > 0.4. For NDVI < 0.4, R_s was relatively constant, probably due to low respiratory activity at low temperatures and thus cannot be captured by variations in NDVI. Furthermore, there were also significant relationships between R_s and MODIS-derived LST and LSTn was found to be a stronger predictor of R_s (Fig. 2b and c). Based on these results, we hypothesized that predicting R_s using the product of NDVI and LSTn would be successful. We found that 8-day-averaged R_s was highly correlated with NDVI × LSTn with $R^2 = 0.86$, $p < 0.001$ (Fig. 2d). In particular, a linear relationship between R_s and NDVI × LSTn would be helpful for improving R_s modeling both at its low and high ends as,

$$R_S = a(\mathrm{NDVI} \times \mathrm{LSTn}) + b \quad (5)$$

where a is the slope and b is the intercept.

3.2. Model calibration using site specific indicators

We calibrated this algorithm, i.e., determining the parameters, a and b in Eq. (5), using site specific indicators. For each year, we correlated 8-day average R_s with NDVI × LSTn using annual data and obtained yearly values of a and b for 2002–2009. Results showed that while the annual value of a was linearly correlated ($R^2 = 0.73$, $p = 0.007$) to annual $\mathrm{LAI}_{\mathrm{max}}$, the annual value of b was linearly correlated ($R^2 = 0.74$, $p = 0.005$) to annual $\mathrm{LAI}_{\mathrm{ave}}$ (Fig. 3).

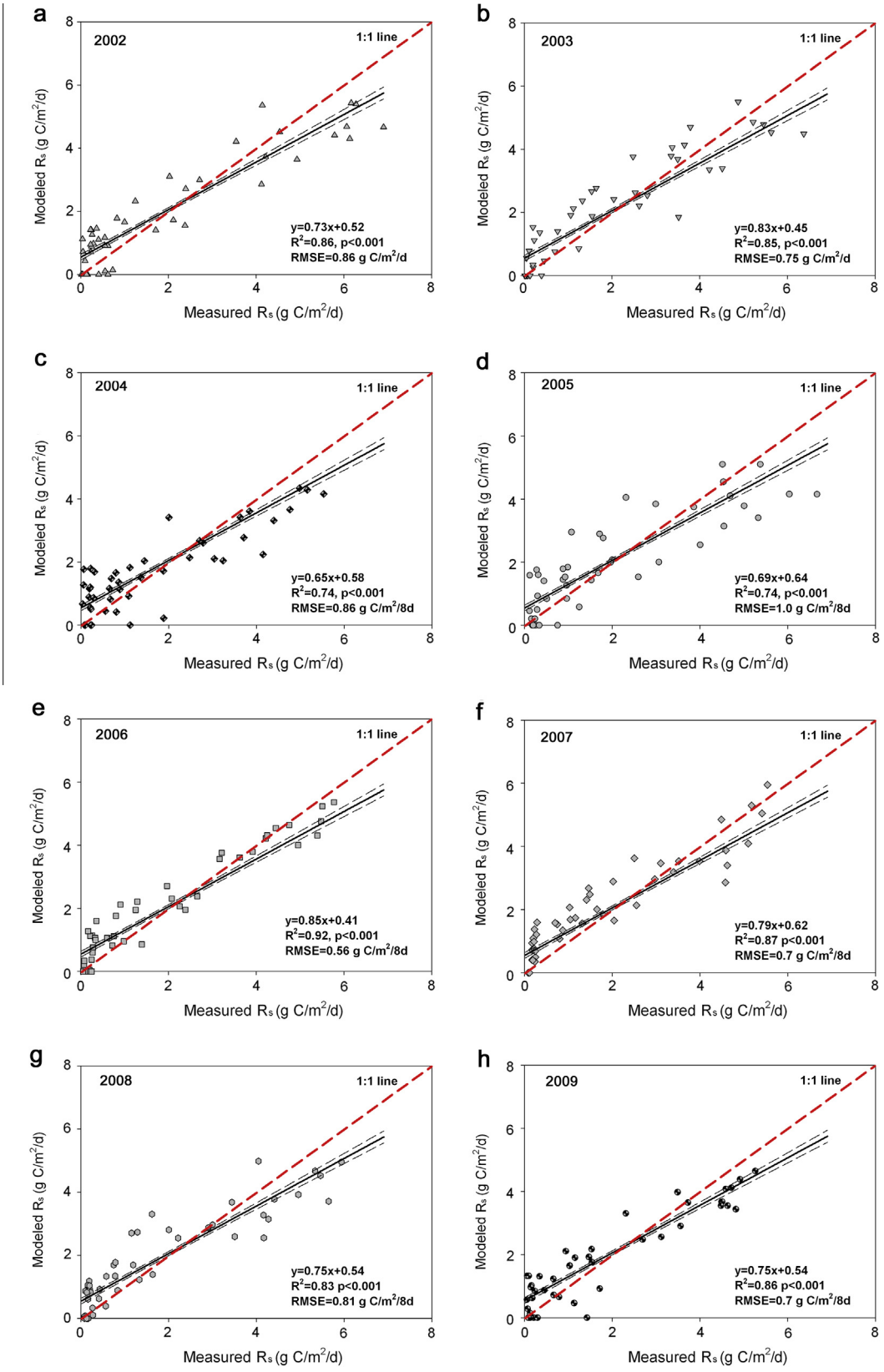

Fig. 5. Relationship between the modeled and measured soil respiration (R_s) at SK-OBS for the years 2002–2009. The dashed lines show the 95% confidence intervals of mean prediction for the regression line.

Therefore, the new model of Eq. (5) with calibration coefficients can be further written as,

$$\begin{aligned} R_S &= a(\mathrm{NDVI} \times \mathrm{LSTn}) + b \\ a &= 0.09\mathrm{LAI}_{max} - 0.01 \\ b &= 1.98\mathrm{LAI}_{ave} - 0.43 \end{aligned} \quad (6)$$

3.3. Modeled soil respiration validation

As expected, a comparison of using Eqs. (5) and (6) to calculate R_s values for each year showed that Eq (6) described the measurements better for each year (Fig. 4). Accordingly, relationships between measured and modeled values of R_s for each year using Eq (6) are shown in Fig. 5. The highest correlation between modeled and measured R_s was observed in 2006 with an R^2 of 0.92 ($p < 0.001$) and the lowest correlation was found for 2004 and 2005 both with an R^2 of 0.74 ($p < 0.001$). For the remaining years, values of R^2 were greater than 0.80, indicating a good performance of this model. The root mean square error of the modeled values varied between 0.6 g C m^{-2} d^{-1} in 2006 and 1.0 g C m^{-2} d^{-1} in 2005.

Model validation using independent measurements at SK-OA and SK-OJP sites was also promising (Fig. 6). We found that for both sites, modeled R_s was significantly correlated with measurements with R^2 of 0.82 ($p < 0.001$) and 0.73 ($p < 0.001$) for SK-OA and SK-OJP, respectively. RMSE for each site was also reasonable. For the combined data of two sites, a significant correlation was found between model estimates and measurements that the model can explain 78% of R_s variance using entirely MODIS data with an RMSE of 1.5 g C m^{-2} d^{-1}.

3.4. Spatial and temporal patterns of mapped R_s

Based on above evaluations, we mapped monthly R_s using entirely MODIS data for forest landscapes of the whole province in 2003 (Fig. 7). Temporal patterns of R_s were well captured that modeled R_s showed clear seasonal evolutions with relatively low simulations in the dormant season (November–March). R_s increased quickly after the start of the growing season and maximized in summer months and then underwent an evident decrease since autumn. Spatial patterns of R_s were also well simulated that broadleaf deciduous forests showed higher R_s than that of the evergreen needleleaf forests. A general decrease patter in R_s was also found from south to north regions, probably because of lower temperature as latitude increases.

4. Discussion

4.1. The role of nighttime LST

The impact of soil temperature on R_s has been intensively investigated. Here we found that the MODIS LST product could be used in models predicting R_s. Our data suggest that LSTn has a greater potential in explaining variations in R_s than LSTd. A possible reason from all data at SK-OBS site is that LSTn is much more resistant to various residual noise components (Fig. 8). We calculated standard deviations of both LSTd and LSTn (i.e., sd_{LSTd} and sd_{LSTn}) from 2002 to 2009 and found that sd_{LSTn} was much lower than sd_{LSTd}, implying the former will reduce noise in the calculated temporal course of R_s. These results may also imply that LSTn could be a better estimate of the baseline temperature that regulates plant phenology (Sims et al., 2008).

4.2. Implications of calibration

We found that the slopes and intercepts of the R_s vs. NDVI × LST_n relationship (i.e., a and b) could be expressed as functions of seasonal LAI_{max} and LAI_{ave}, respectively. The slopes should ideally represent the rate at which R_s increases with per unit NDVI × LSTn. Since R_s consists of both microbially and root-respired C, it should be dependent directly on the input of carbon from living plants (Moyano et al., 2008). This likely explains why a was found to be significantly correlated with LAI_{max}, since it partly determines the amount of carbohydrates that are transferred from leaves to the rhizosphere. This is consistent with the results of Janssens et al. (2001) that productivity (LAI being a proxy for it in this study) is tied to R_s since the availability of organic matter (leaves, fine roots) for respiration depends on primary productivity. The value of b may not have specific physiological indications and is simply the value of R_s at an LST_n of zero. One significant contribution of our analysis is that the calibration approach (i.e., using statistics of LAI to determine regression coefficients) works well for the other two independent sites, suggesting the general suitability of our algorithm to estimate R_s across plant functional types. This probably could be a great advantage towards the exploration of spatial patterns of R_s using remote sensing in future.

4.3. Factors influencing model performance

To better explain the interannual behavior of model performance, using long-term data at SK-OBS site, we found that the value of R^2 between R_s and NDVI × LST_n was negatively correlated with the standard deviation of SWC (sd_{SWC}) while being positively correlated with the standard deviation of LAI (sd_{LAI}) (Fig. 9). The relationship between R^2 and sd_{SWC} suggests that our model is affected by soil water status, which has been recognized as a quite challenging task from optical remote sensing (Albergel et al., 2012). Larger values of sd_{SWC} in SK-OBS appeared to be the result of above-average precipitation during the growing season. For example, a value of sd_{SWC} of 14.3% was observed in 2004, when the growing season precipitation was 30% above the 8-year average. A similar condition was also observed in 2005 (sd_{SWC} of 11.2%). For these two years, NDVI × LST_n was only able to explain 71% and 72% of the variance in R_s, respectively. For severe drought years, e.g., 2003, NDVI × LST_n also had a moderate accuracy in estimating R_s. The highest ability of NDVI × LSTn to explain R_s (R^2 = 0.92) was found in 2006, a year with slightly high annual precipitation (5% above average). These results imply that the SWC

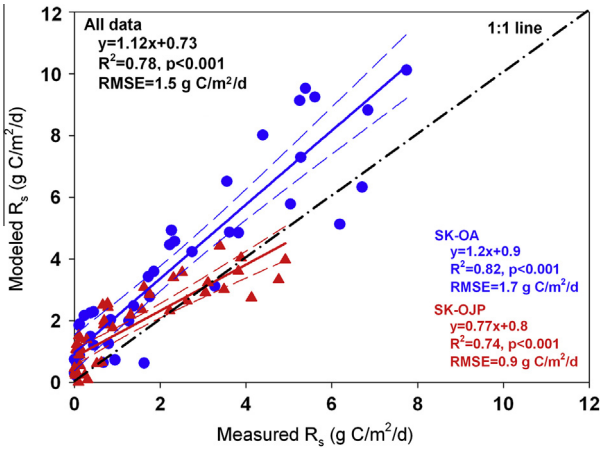

Fig. 6. Comparison between modeled and measured R_s at SK-OA (●) and SK-OJP (▲) sites using the algorithm proposed at SK-OBS site. The dashed lines show the 95% confidence intervals of mean prediction for the regression line.

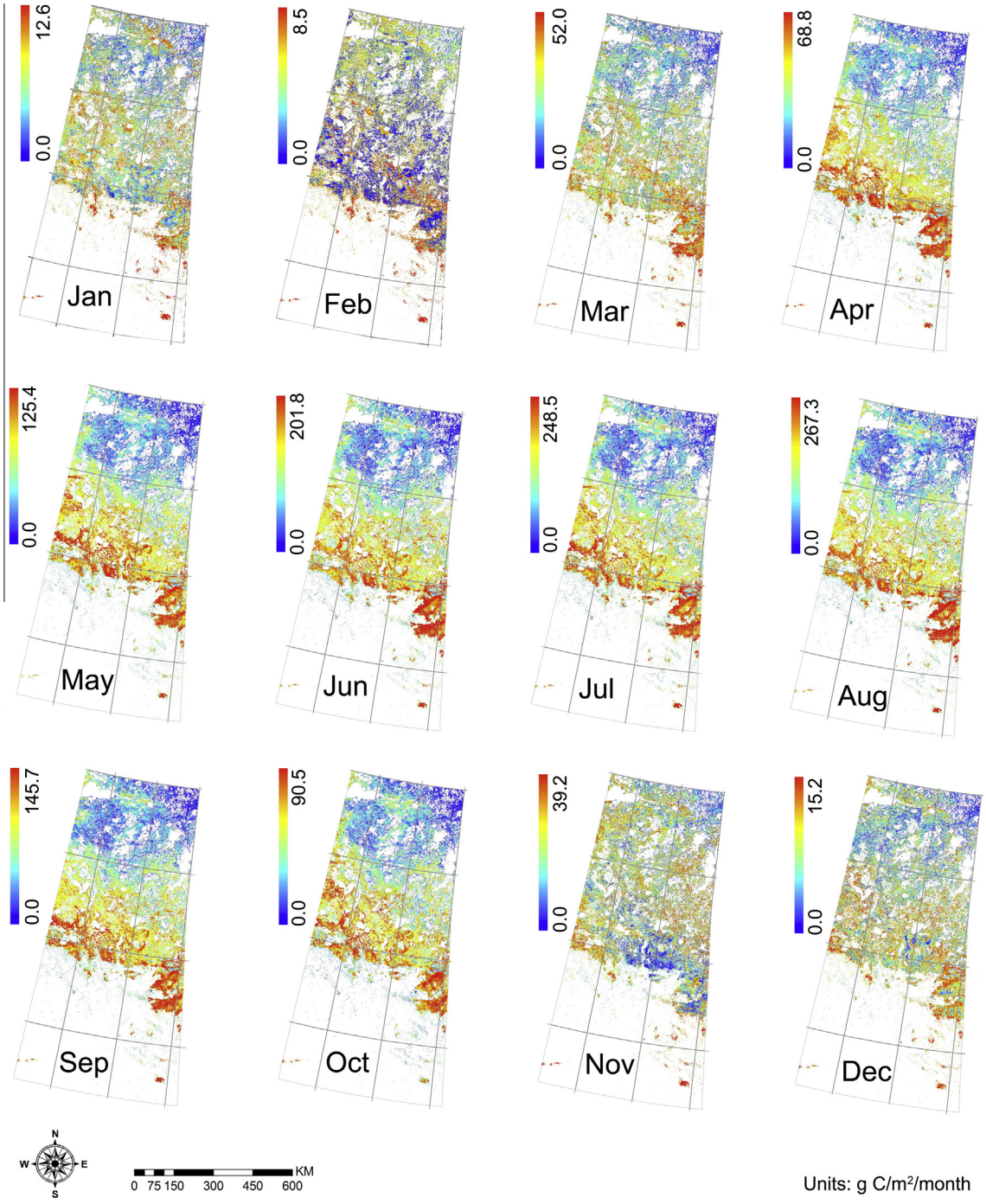

Fig. 7. Simulations of monthly soil respiration (R_s) of forest landscapers of Saskatchewan, Canada using MODIS data in 2003.

may have competing effects on model performance, so that our algorithm still performed moderately well in capturing variations in R_s under these conditions. A complicated relationship between soil water status and ecosystem functioning will make modeling R_s challenging in either extremely wet or droughty conditions (Wu et al., 2013b). Analysis aimed at partitioning R_s into its autotrophic and heterotrophic components may be a potential way to better understand the response of R_s to SWC (Moyano et al., 2013). This agrees with findings reported in Gaumont-Guay et al. (2014) that SWC alone was only able to explain 18% of R_s variations and may also explain that even without considering water status in the algorithm, our approach still has the potential to capture the first order of spatial and temporal variations of R_s. Better model performances for years with large variations in LAI may simply be a reflection that the model would give better results under favorable growth conditions because larger sd_{LAI} is associated with higher seasonal LAI_{max}.

4.4. Temporal and spatial constrains of the model

Temporal and spatial constrains of the model should be highlighted to address its sensitivity with respect to sampling size and temporal resolution. Our algorithm is proposed at 8-day temporal scale, and this excludes the interface from seasonality. For

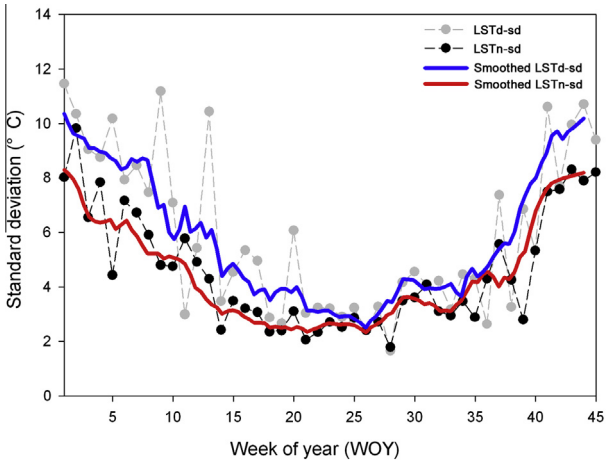

Fig. 8. Seasonal variations of the standard deviation (sd) of daytime (LST_d; grey dots and dashed line) and nighttime (LST_n; black dots and dashed line) land surface temperatures from 2002 to 2009. Also shown are smoothed lines for sd of LST_d (blue) and LST_n (red), respectively. (For interpretation of the references to color in this figure legend, the reader is referred to the web version of this article.)

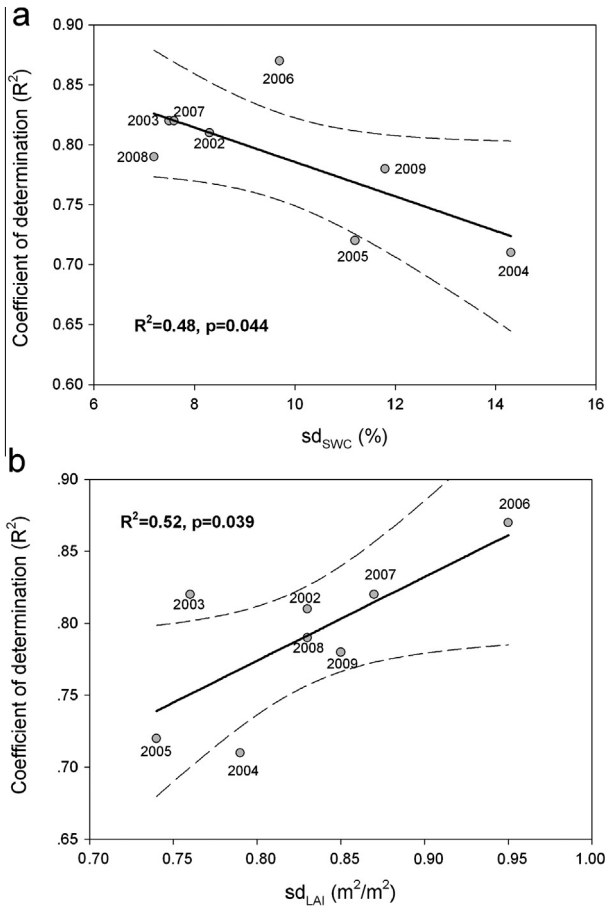

Fig. 9. Relationships between the coefficient of determination (R^2), and (a) the standard deviation of volumetric soil water content (sd_{SWC}) and (b) the standard deviation of leaf area index (sd_{LAI}). The dashed lines show the 95% confidence intervals of mean prediction for the regression line.

example, the good model performance would be definitely influenced by vegetation seasonality at monthly temporal scale. However, if we can demonstrate the model at 8-day period, such concern can be resolved. For the spatial aspect, we only have validation data at flux tower sites and this limits the resolution to 1 km. Currently, it might be impossible to analyze the spatial sensitivity since there is no ground data to support such experiment. Therefore, the confidence of spatial patterns of Rs modeled is based on the results shown in Figs. 5 and 6. Consequently, it is difficult to show the areas with low correlations because of data availability. Overall, our analysis is focused on the development of new models for soil respiration modeling and to link the model with semi-physical explanations. Technical issues related to computational ability and algorithm portability are not concerned at present.

4.5. Potentials and implications for remote sensing of R_s

Remote sensing data provide a real opportunity to robustly test predictions of R_s with respect to changes in controlling factors for large spatial extent and sample size. We found that R_s was correlated with NDVI. However, NDVI alone is not able to explain variations in R_s very well, especially considering the relatively constant values of R_s for NDVI < 0.4 at SK-OBS site (Fig. 2a). This feature potentially suggests that NDVI may only provide useful signals of R_s during the growing season when photosynthesis is active. For dormant seasons when photosynthesis is limited by low temperature, NDVI is no longer an indicator of R_s, which is largely controlled by soil temperature. Thus, results of recently reported relationships between R_s and spectral vegetation index in Huang et al. (2012) should be viewed with caution because only measurements of two crops during the growing season were included. Here we showed high precision in predicting R_s by combining NDVI and LST_n and the model also showed promising validation at independent sites with different plant functional types. By combine both NDVI and LSTn, our model still reasonably reproduced R_s both for the growing season and the dormant season. Though there was overestimation of R_s at its low range (Fig. 5), improvements can be achieved compared with the NDVI-only estimation. By including LSTn, we can partly mitigate the strong dependence on the quality of NDVI. For example, even when NDVI is contaminated by the presence of snow in winter, restriction from low LSTn can still provide reasonable estimates of R_s. One potential way to solve this problem would be the separation of growing and dormant seasons, which might require a new module to determine the time of growing season start and end. This might not be easily determined using empirical approach of temperature because of large interannual variability of growing season length reported at these sites (Wu et al., 2013a). Furthermore, this may also lead to additional variables that make our approach not entirely driven by remote sensing observations.

Our results mainly contribute to our understanding in two aspects. First, it confirms that belowground activities, to some degree, can be linked to aboveground photosynthesis, supporting the claim that R_s is an indicator of plant metabolism (Moyano et al., 2008; Caquet et al., 2012). However, this linkage may be time dependent and is only valid within the growing season. More importantly, since NDVI and LST_n can be acquired by satellite data, this method has the potential to be upscaled regionally or even globally after rigorous calibrations among other plant functional types (e.g., crops and grasslands). Therefore, it will provide a unique way to analyze the response of R_s to climate change spatially and temporally, considering the long term records of NDVI going back to late the 70s of the last century.

5. Conclusions

The availability of automated soil respiration measurements provides sub-hourly information to observe short-term variation in soil respiration and allows for better understanding of the controls of soil respiration across various temporal scales. An eight-

year continuous soil CO_2 efflux was measured at a boreal black spruce stand and a new approach was proposed to predict 8-day average R_s using solely MODIS observations. Additional validation at other two sites of different plant functional types was also successful, indicating high level of portability of the new model. Spatial and temporal patterns of R_s for all forested areas in Saskatchewan were well captured using the model we proposed, representing a potential way to upscale R_s from site level measurements to regional scale. These results suggest the close linkage between the processes of photosynthesis and respiration. In particular, we have shown the potential of satellite data in the estimation of R_s, which would be a valuable tool in the exploration of the spatio-temporal characteristics of *Rs* in future climate change scenarios. Further analysis would involve the application of this model at more sites in diverse ecoregions and calibration across various plant functional types (e.g., grasslands, savannas).

Acknowledgements

This study was funded by an NSERC Strategic Grant (381474-09) and the National Natural Science Foundation of China (Grant No. 41371013, 41271412). The flux and climate measurements were made as part of the Fluxnet Canada Research Network and the Canadian Carbon Program (through NSERC, the Canadian Foundation for Climate and Atmospheric Sciences (CFCAS), BIOCAP Canada) and the Meteorological Service of Canada through a Contribution Agreement to the University of British Columbia. The authors sincerely acknowledge the technical assistance of Zoran Nesic, Nick Grant, Andrew Sauter and Dominic Lessard, the help of various contractors as well as employees of the Meteorological Service of Canada for system maintenance and data acquisition and the strong support from Alan Barr. The 2005 North American Land Cover at 250 m spatial resolution was produced by Natural Resources Canada/Canadian Centre for Remote Sensing (NRCan/CCRS), United States Geological Survey (USGS); Insituto Nacional de Estadística y Geografía (INEGI), Comisión Nacional para el Conocimiento y Uso de la Biodiversidad (CONABIO) and Comisión Nacional Forestal (CONAFOR).

References

Albergel, C., de Rosnay, P., Gruhier, C., Muñoz-Sabater, J., Hasenauer, S., Isaksen, L., Kerr, Y., Wagner, W., 2012. Evaluation of remotely sensed and modelled soil moisture products using global ground-based in situ observations. Remote Sens. Environ. 118, 215–226.

Bahn, M., Reichstein, M., Davidson, E.A., Grünzweig, J., Jung, M., Carbone, M.S., et al., 2010. Soil respiration at mean annual temperature predicts annual total across vegetation types and biomes. Biogeosciences 7, 2147–2157.

Barr, A.G., Black, T.A., Hogg, E.H., Kljun, N., Morgenstern, K., Nesic, Z., 2004. Interannual variability in the leaf area index of a boreal aspen-hazelnut forest in relation to net ecosystem production. Agr. Forest Meteorol. 126 (3–4), 237–255.

Bisbee, K.E., Gower, S.T., Norman, J.M., Nordheim, E.V., 2001. Environmental controls on ground cover species composition and productivity in a boreal black spruce forest. Oecologia 129 (2), 261–270.

Black, T.A., Chen, W.J., Barr, A.G., Arain, M.A., Chen, Z., Nesic, Z., Hogg, E.H., Neumann, H.H., Yang, P.C., 2000. Increased carbon sequestration by a boreal deciduous forest in years with a warm spring. Geophys. Res. Lett. 27 (9), 1271–1274.

Blonquist Jr., J.M., Jones, S.B., Robinson, D.A., 2006. Precise irrigation scheduling for turfgrass using a subsurface electromagnetic soil moisture sensor. Agr. Water Manage. 84 (1–2), 153–165.

Bond-Lamberty, B., Thomson, A., 2010. Temperature-associated increases in the global soil respiration record. Nature 464 (7288), 579–582.

Bond-Lamberty, B., Bunn, A.G., Thomson, A.M., 2012. Multi-year lags between forest browning and soil respiration at high northern latitudes. PLoS ONE 7, e50441. http://dx.doi.org/10.1371/journal.pone.0050441.

Caquet, B., De Grandcourt, A., M'bou, A.T., Epron, D., Kinana, A., André, L.S., Nouvellon, Y., 2012. Soil carbon balance in a tropical grassland: estimation of soil respiration and its partitioning using a semi-empirical model. Agr. Forest Meteorol. 158, 71–79.

Chen, B., Coops, N.C., Fu, D., Margolis, H.A., Amiro, B.D., Barr, A.G., et al., 2011. Assessing eddy-covariance flux tower location bias across the Fluxnet-Canada Research Network based on remote sensing and footprint modelling. Agr. Forest Meteorol. 151 (1), 87–100.

Chen, J.M., Rich, P.M., Gower, S.T., Norman, J.M., Plummer, S., 1997. Leaf area index of boreal forests: theory, techniques, and measurements. J. Geophys. Res. 102 (D24), 29429–29443.

Davidson, E.A., Janssens, I.A., Luo, Y., 2006. On the variability of respiration in terrestrial ecosystems: moving beyond Q_{10}. Global Change Biol. 12 (2), 154–164.

Dunn, A.L., Barford, C.C., Wofsy, S.C., Goulden, M.L., Daube, B.C., 2007. A long-term record of carbon exchange in a boreal black spruce forest: means, responses to interannual variability and decadal trends. Global Change Biol. 13 (3), 577–590.

Ekblad, A., Boström, B., Holm, A., Comstedt, D., 2005. Forest soil respiration rate and $\delta^{13}C$ is regulated by recent above ground weather conditions. Oecologia 143 (1), 136–142.

Gaumont-Guay, D., Black, T.A., Barr, A.G., Griffis, T.J., Jassal, R.S., Krishnan, P., Grant, N., Nesic, Z., 2014. Eight years of forest-floor CO_2 exchange in a boreal black spruce forest: spatial integration and multi-temporal trends. Agr. Forest Meteorol. 184, 25–35.

Gaumont-Guay, D., Black, T.A., Griffis, T.J., Barr, A.G., Jassal, R.S., Nesic, Z., 2006. Interpreting the dependence of soil respiration on soil temperature and water content in a boreal aspen stand. Agr. Forest Meteorol. 140 (1–4), 220–235.

Gaumont-Guay, D., Black, T.A., McCaughey, H., Barr, A.G., Krishnan, P., Jassal, R.S., Nesic, Z., 2009. Soil CO_2 efflux in contrasting boreal deciduous and coniferous stands and its contribution to the ecosystem carbon balance. Glob. Change Biol. 15 (5), 1302–1319.

Griffis, T.J., Black, T.A., Baumont-Guay, D., Drewitt, G.B., Nesic, Z., Barr, A.G., Morgenstern, K., Kljun, N., 2004. Seasonal variation and partitioning of ecosystem respiration in a southern boreal aspen forest. Agr. Forest Meteorol. 125 (3–4), 207–223.

Högberg, P., Nordgren, A., Buchmann, N., Taylor, A.F.S., Ekblad, A., Högberg, M.N., Nyberg, G., Ottosson-Löfvenius, M., Read, D.J., 2001. Large-scale forest girdling shows that current photosynthesis drives soil respiration. Nature 411 (6839), 789–792.

Huang, N., Niu, Z., Zhan, Y., Xu, S., Tappet, M.C., Wu, C., et al., 2012. Relationships between soil respiration and photosynthesis-related spectral vegetation indices in two cropland ecosystems. Agr. Forest Meteorol. 160, 80–89.

Janssens, I.A., Lankreijer, H., Matteucci, G., Kowalski, A.S., Buchmann, N., Epron, D., et al., 2001. Productivity overshadows temperature in determining soil and ecosystem respiration across European forests. Global Change Biol. 7 (3), 269–278.

Jassal, R.S., Black, T.A., Drewitt, G.B., Novak, M.D., Gaumont-Guay, D., Nesic, Z., 2004. A model of the production and transport of CO_2 in soil: Predicting soil CO_2 concentrations and CO_2 efflux from a forest floor. Agr. Forest Meteorol. 124 (3–4), 219–236.

Jassal, R., Black, A., Novak, M., Morgenstern, K., Nesic, Z., Gaumont-Guay, D., 2005. Relationship between soil CO_2 concentrations and forest-floor CO_2 effluxes. Agr. Forest Meteorol. 130 (3–4), 176–192.

Jassal, R.S., Black, T.A., Nesic, Z., 2012a. Biophysical controls of soil CO_2 efflux in two coastal Douglas-fir stands at different temporal scales. Agr. Forest Meteorol. 153, 134–143.

Jassal, R.S., Black, T.A., Nesic, Z., Gaumont-Guay, D., 2012b. Using automated non-steady-state chamber systems for making continuous long-term measurements of soil CO_2 efflux in forest ecosystems. Agr. Forest Meteorol. 161, 57–65.

Justice, C.O., Townshend, J.R.G., Vermote, E.F., Masuoka, E., Wolfe, R.E., Saleous, N., Roy, D.P., Morisette, J.T., 2002. An overview of MODIS Land data processing and product status. Remote Sens. Environ. 83 (1–2), 3–15.

Kuzyakov, Y., Gavrichkoa, O., 2010. Time lag between photosynthesis and carbon dioxide efflux from soil: a review of mechanisms and controls. Global Change Biol. 16 (12), 3386–3406.

Mahecha, M.D., Reichstein, M., Carvalhais, N., Lasslop, G., Lange, H., Seneviratne, S.I., et al., 2011. Response to comment on "global convergence in the temperature sensitivity of respiration at ecosystem level". Science 331 (5993), 1265.

Mitrakis, N.E., Mallinis, G., Koutsias, N., Theocharis, J.B., 2012. Burned area mapping in Mediterranean environment using medium-resolution multi-spectral data and a neuro-fuzzy classifier. Inter. J. Image Data Fusion 3 (4), 299–318.

Moyano, F.E., Kutsch, W.L., Rebmann, C., 2008. Soil respiration fluxes in relation to photosynthetic activity in broad-leaf and needle-leaf forest stands. Agr. Forest Meteorol. 148 (1), 135–143.

Moyano, F.E., Manzoni, S., Chenu, C., 2013. Responses of soil heterotrophic respiration to moisture availability: an exploration of processes and models. Soil Biol. Biochem. 59, 72–85.

Myneni, R.B., Hoffman, S., Knyazikhin, Y., Privette, J.L., Glassy, J., Tian, Y., et al., 2002. Global products of vegetation leaf area and fraction absorbed PAR from year one of MODIS data. Remote Sens. Environ. 83 (1–2), 214–231.

Ngao, J., Epron, D., Delpierre, N., Bréda, N., Granier, A., Longdoz, B., 2012. Spatial variability of soil CO_2 efflux linked to soil parameters and ecosystem characteristics in a temperate beech forest. Agr. Forest Meteorol. 154, 136–146.

Reichstein, M., Rey, A., Freibauer, A., Tenhunen, J., Valentini, R., Banza, J., et al., 2003. Modeling temporal and largescale spatial variability of soil respiration from soil water availability, temperature and vegetation productivity indices. Global Biogeoch. Cycle 17 (4), 1–15.

Sims, D.A., Rahman, A.F., Cordova, V.D., El-Masri, B.Z., Baldocchi, D.D., Bolstad, P.V., et al., 2008. A new model of gross primary productivity for North American ecosystems based solely on the enhanced vegetation index and land surface temperature from MODIS. Remote Sens. Environ. 112 (4), 1633–1646.

Trumbore, S., 2006. Carbon respired by terrestrial ecosystems-recent progress and challenges. Global Change Biol. 12 (2), 141–153.
Valentini, R., Matteucci, G., Dolman, A.J., Schulze, E.D., Rebmann, C., Moors, J., et al., 2000. Respiration as the main determinant of carbon balance in European forests. Nature 404 (6780), 861–865.
Wan, Z., 2008. New refinements and validation of the MODIS land-surface temperature/emissivity products. Remote Sens. Environ. 112 (1), 59–74.
Wu, C., Chen, J.M., Huang, N., 2011. Predicting gross primary production from the enhanced vegetation index and photosynthetically active radiation: evaluation and calibration. Remote Sens. Environ. 115 (15), 3424–3435.
Wu, C., Chen, J.M., Desai, A.R., Hollinger, D.Y., Arain, M.A., Margolis, H.A., Gough, C.M., Staebler, R.M., 2012. Remote sensing of canopy light use efficiency in temperate and boreal forests of North America using MODIS imagery. Remote Sens. Environ. 118, 60–72.
Wu, C., Chen, J.M., Desai, A.R., Lafleur, P.M., Verma, S.B., 2013a. Positive impacts of precipitation intensity on monthly CO_2 fluxes in North America. Global Planet. Change 100, 204–214.
Wu, C., Chen, J.M., Black, T.A., Price, D.T., Kurz, W.A., Desai, A.R., et al., 2013b. Interannual variability of net ecosystem productivity in forests is explained by carbon flux phenology in autumn. Global Ecology Biogeog. 22 (8), 994–1006.
Wu, C., Gonsamo, A., Gough, C.M., Chen, J.M., Xu, S., 2014. Modeling growing season phenology of North American forests using seasonal mean vegetation indices from MODIS. Remote Sens. Environ. 147, 79–88.
Xiao, X., Zhang, Q., Braswell, B., Urbanski, S., Boles, S., Wofsy, S., Moore III, B., Ojima, D., 2004. Modeling gross primary production of temperate deciduous broadleaf forest using satellite images and climate data. Remote Sens. Environ. 91 (2), 256–270.
Zhang, Q., Middleton, E.M., Margolis, H.A., Drolet, G.G., Barr, A.G., Black, T.A., 2009. Can a satellite-derived estimate of the fraction of PAR absorbed by chlorophyll (FAPARchl) improve predictions of light-use efficiency and ecosystem photosynthesis for a boreal aspen forest? Remote Sens. Environ. 113 (4), 880–888.
Yuan, W.P., Luo, Y.Q., Richardson, A.D., Oren, R., Luyssaert, S., Janssens, I.A., et al., 2009. Latitudinal patterns of magnitude and interannual variability in net ecosystem exchange regulated by biological and environmental variables. Global Change Biol. 15 (12), 2905–2920.
Zhu, X., Toutin, T., 2013. Land cover classification using airborne LiDAR products in Beauport, Québec, Canada. Inter. J. Image Data Fusion 4 (3), 252–271.